ORIGINAL PAPER

Cyclostratigraphic dating in the Lower Badenian (Middle Miocene) of the Vienna Basin (Austria): the Baden-Sooss core

J. Hohenegger · S. Ćorić · M. Khatun · P. Pervesler · F. Rögl · C. Rupp · A. Selge · A. Uchman · M. Wagreich

Abstract The scientific borehole Baden-Sooss penetrates a succession of Badenian (Langhian, Middle Miocene) sediments at the type locality of the Badenian, the old brickyard Baden-Sooss in the Vienna Basin. The sedimentary succession of the 102-m-cored interval consists of more than 95% bioturbated, medium-to-dark gray marly shales with carbonate contents between 11 and 25% and organic carbon contents between 0.35 and 0.65%. Biostratigraphic investigations on foraminifera (mainly lower part of Upper Lagenid Zone) and calcareous nannoplankton (standard zone NN5) indicate an early Badenian (Langhian) age. Cycles in carbonate content, organic carbon content, and magnetic susceptibility have been identified by power spectra analysis. Correlations between the three variables are extremely significant. Using cross-correlation, periods around 40 m correlate significantly with the 100 kyr^{-1} eccentricity cycle, the ∼20 m periods with the obliquity cycle, and the 15 to 11-m periods with both precession cycles. Wavelet transformation and decomposition of composite periodic functions were used to obtain the position of the cycle peaks in the profile. Cross-correlation with orbital cycles (La2004) dates the Baden-Sooss core between -14.379 ± 1 and -14.142 my ± 9 kyr.

Introduction

The Vienna Basin constitutes a classical area of geological and paleontological investigations of Miocene strata. The basin is situated at the junction of the Eastern Alps and the Western Carpathians (e.g. Decker 1996; Hamilton et al. 2000; see Fig. 1) and formed during Neogene lateral extrusion within the Eastern Alps (Ratschbacher et al. 1991; Decker 1996).

A wealth of data for the Vienna Basin has been gathered by the oil industry, mainly OMV AG. Due to the bad outcrop situation, however, detailed sedimentological and paleontological investigations are restricted to a few natural outcrops and a handful of active pits. Therefore, a scientific borehole was drilled in 2003 near the western margin of the southern Vienna Basin. The aim was a detailed sampling of a longer succession of Miocene sediments. The scientific borehole Baden-Sooss penetrated a succession of Badenian (Langhian, Middle Miocene) deposits, starting from the type section of the Badenian stage, the old brickyard Baden-Sooss near Baden (Papp et al. 1978; see Fig. 1). The whole 102 m of the Baden-Sooss borehole were cored for the application of multidisciplinary methods, including

J. Hohenegger (✉) · P. Pervesler
Department of Palaeontology,
University of Vienna, Vienna, Austria
e-mail: johann.hohenegger@univie.ac.at

S. Ćorić · C. Rupp
Geological Survey of Austria, Vienna, Austria

M. Khatun · M. Wagreich
Department of Geodynamics and Sedimentology,
University of Vienna, Vienna, Austria

F. Rögl
Natural History Museum Vienna, Vienna, Austria

A. Selge
Paleomagnetic Laboratory Gams,
Institute of Geophysics, MU Leoben, Austria

A. Uchman
Institute of Geological Sciences, Jagiellonian University,
Oleandry 2a, 30-063 Kraków, Poland

Fig. 1 **a** Tectonic sketch map of the Vienna Basin (modified from Decker 1996; Wagreich and Schmid 2002) and location of the studied borehole Baden-Sooss. **b** Schematic sedimentological log of the borehole Baden-Sooss from 6 to 102 m
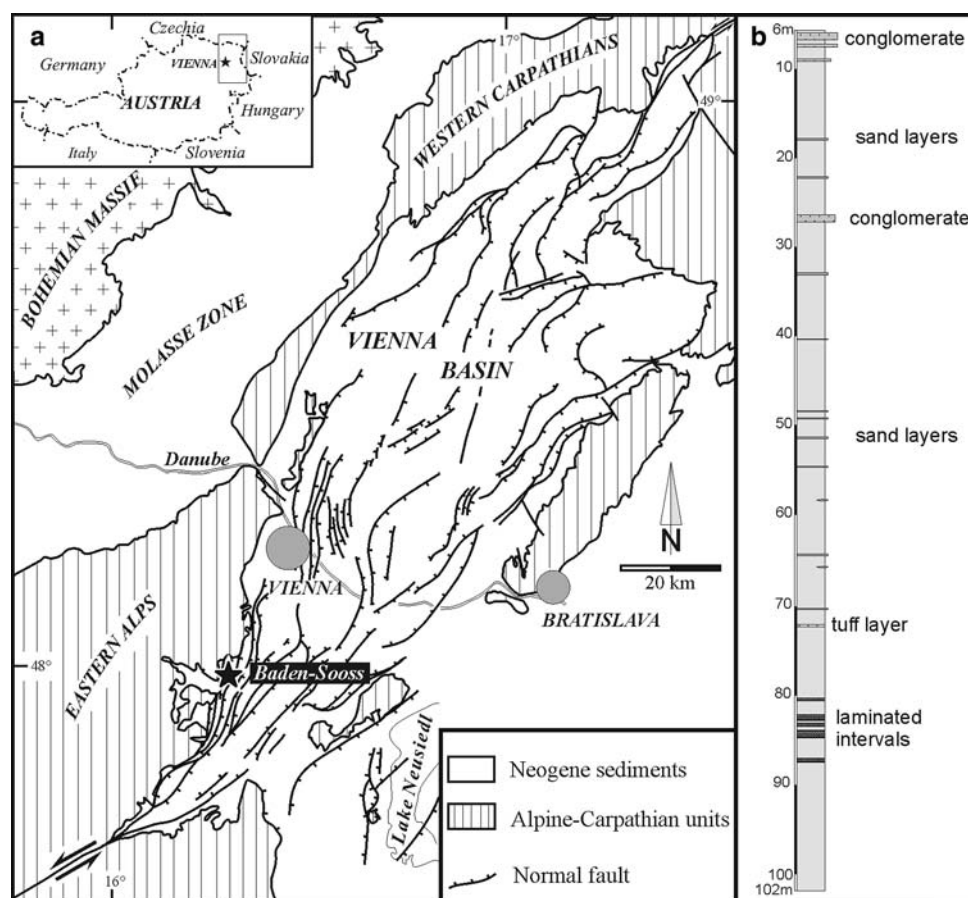
biostratigraphy, paleoecology, paleoichnology, sedimentology, geochemistry, magnetostratigraphy, and paleoclimatology (Baldi et al. 2005; Selge 2005; Kathun et al. 2005). The high resolution of the core was designed to allow age determination by comparing cyclicity in geochemical and geomagnetic parameters with orbital cycles using phase relations for astronomical tuning (e.g. Hilgen et al. 1995; 2000; Abels et al. 2005).

Geological setting

The Vienna Basin (Fig. 1a), a part of the Neogene Paratethys basin system (Steininger and Wessely 2000), constitutes a complex pull-apart basin on top of thrust sheets of the Eastern Alps and the Carpathians. The structural evolution of the Vienna Basin is characterized by successive phases of compression, strike-slip movements, and extension, related to orogenic compression and lateral extrusion (Ratschbacher et al. 1991; Decker and Peresson 1996; Strauss et al. 2006).

The evolution of the Vienna Basin started during the Early Miocene with the development of a partly non-marine piggyback basin on top of Alpine thrusts to the northeast of today's Vienna (Hamilton et al. 2000). Sinistral transtension during the Early/Middle Miocene led to the formation of small-scale, rapidly subsiding lows and relatively stable highs during the Badenian and Sarmatian. A renewed marine transgression started in the Early Badenian. Up to 3,000-m-thick successions of Badenian marls and sandstones characterize the central parts of the basin, whereas delta sands and carbonates were deposited at the basin margins or at shallow depths (Sauer et al. 1992; Weissenbäck 1996; Seifert 1996). During Sarmatian and Pannonian times, salinity oscillated (Piller and Harzhauser 2005) and finally decreased, leading to limnic-fluvial deposits.

The western margin of the southern Vienna Basin is characterized by large normal or oblique faults that displace marginal sediments such as deltaic deposits and shallow-marine limestones ("Leithakalk") against basinal fine-grained strata ("Tegel"). In the old brickyard Baden-Sooss, faults that displace Badenian against Sarmatian strata are visible (e.g. Papp and Steininger 1978: Fig. 30). Poor outcrops (preserved as a "Naturdenkmal/natural monument" at the margin of the waste-disposal site Sooss) and descriptions from the literature indicate the presence of fine-grained marls and clays with minor sand layers and mollusk-bearing lenses.

Stratigraphy

The lithostratigraphic division of Badenian sediments in the Austrian part of the basin is still under debate. During the nineteenth and the first half of the twentieth century, only the term "mariner Tegel von Baden" was in use. The revision of Austrian Neogene stratigraphic nomenclature (Papp et al. 1968) for the marine Middle Miocene sediments of the Vienna Basin introduced the stratigraphic term "Badener Serie" as a formation. A clear differentiation between litho-, bio-, and chronostratigraphy was not given. The recent lithostratigraphic chart of Austria (Piller et al. 2004) places the "Badener Tegel" into the Baden Group, which can be subdivided into the Jakubov Formation and the Lanžhot Formation in the Slovakian part of the basin. The lower part of the Badenian with the Baden-Sooss borehole may thus be correlated to the Lanžhot Formation (e.g. Kováč et al. 2004) (Fig. 2).

The Vienna Basin has been an important place for the biostratigraphic subdivision of the Neogene in the Parathys, based mainly on mollusk assemblages. An early subdivision was given by Fuchs (1873) into "I and II Mediterranstufe", corresponding to the Early and Middle Miocene. Schaffer (1927) correlated the units with the Mediterranean stages of Mayer-Eymar (1858), introducing

"Tortonian" for the marine Middle Miocene. A new stages system for the Central Parathys was proposed, with the new stage "Badenian" for the marine Middle Miocene (Cicha and Senes 1968; Papp et al. 1968), based on the stratotype section of the brickyard of Baden-Sooss (Papp and Steininger 1978). Based on oil exploration wells in the Vienna Basin, a subdivision of the Badenian based on foraminiferal assemblages was given by Grill (1941, 1943) and subsequently modified by Papp and Turnovsky (1953):

Rotalia Zone or Impoverished Zone (uppermost Badenian)
Bulimina-Bolivina Zone
Zone of agglutinated foraminifera (also termed *Spiroplectammina* Zone)
Upper Lagenid Zone
Lower Lagenid Zone (lower Badenian)

In the description of the Badenian stratotype (Papp and Steininger 1978), the fossil content of the Baden clay ("Badener Tegel") was presented, including the calcareous nannoplankton marker species *Sphenolithus heteromorphus* Deflandre, *Helicosphaera carteri* (Wallich) Kamptner, *Discoaster exilis* Martini and Bramlette, *D. formosus* Martini and Worsley. Based on the occurrences of *S. heteromorphus* Deflandre, Fuchs and Stradner (1977)
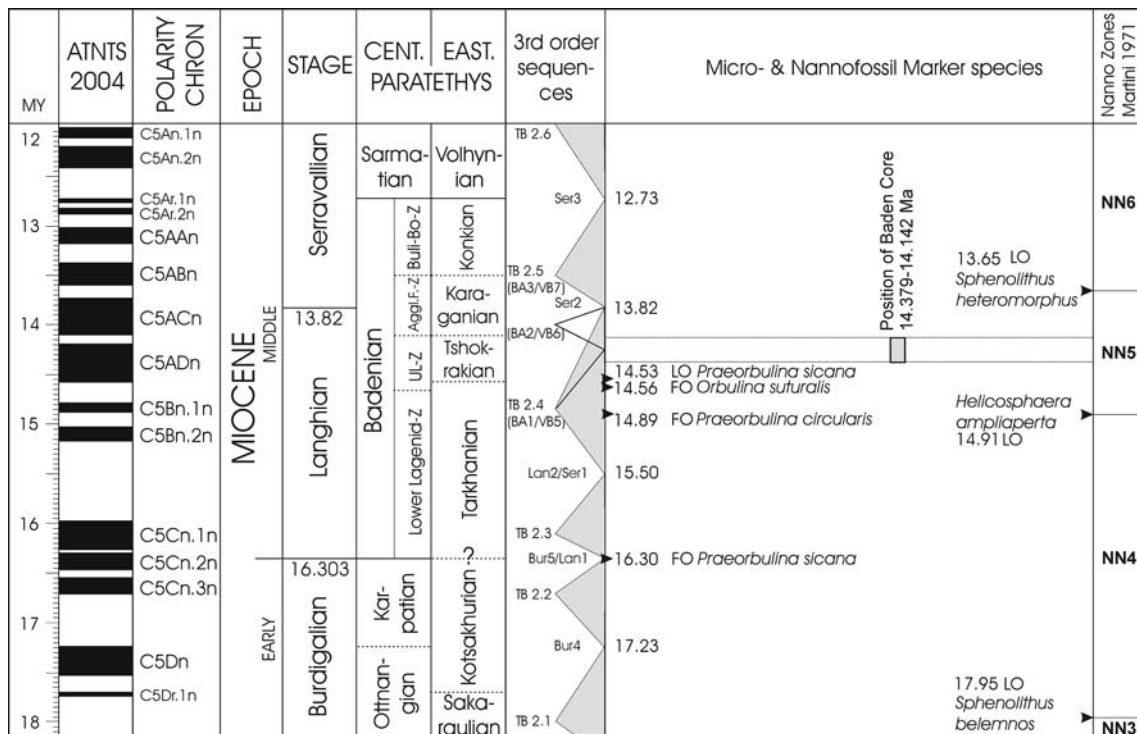
Fig. 2 Lower to Middle Miocene stratigraphic chart, including calibrated planktonic events by Lourens et al. (2004b) and Abdul Aziz et al. (2007), based on the time scale of Lourens et al. (2004a); *FO* first occurrence, *LO* last occurrence. Base of Langhian according to the FO of *Praeorbulina sicana*, acc. to EEDEN project at the base of chron C5Cn.1r. Base of Serravallian at 13.82 My was proposed by Abels et al. (2005). Third-order sequences of Haq et al (1988) are recalibrated according to ATNTS. Vienna Basin cycles are indicated: VB 5-7 of Kováč et al. (2004) and BA 1–3 of Strauss et al. (2006)

attributed rich calcareous nannoplankon assemblages from a nearby drilling at Vöslau to the NN5 Zone (*S. heteromorphus* Zone of Martini, 1971). Stradner and Fuchs (1978) confirmed this attribution on material from several Badenian outcrops in the Vienna Basin, including the brickyard Baden-Sooss. According to Papp and Steininger (1978), the foraminifera *Orbulina suturalis* Brönnimann, *Uvigerina grilli* Schmid, and *Bolivina viennensis* Marks from the Badenian stratotype indicate the Upper Lagenid Zone.

Calcareous nannoplankton

Miocene sediments from the Baden-Sooss core generally contain rich and well-preserved calcareous nannofossil assemblages. The biostratigraphically important marker species *S. heteromorphus* is very scarce but present in the investigated samples. The absence of *H. ampliaperta* and the scarce presence of *S. heteromorphus* indicate nannoplankton Zone NN5 of Martini (1971). The accompanying assemblage is characterized by high percentages of small reticulofenestrids (*Reticulofenestra minuta* Roth and *R. haqii* Backman). The following species regularly occur: *Coccolithus pelagicus* (Wallich) Schiller, *Coronocyclus nitescens* (Kamptner) Bramlette and Wilcoxon, *Cyclicargolithus floridanus* (Roth and Hay) Bukry, helicoliths [*Helicosphaera carteri* (Wallich) Kamptner, *H. walbersdorfensis* Müller], *Pontosphaera multipora* (Kamptner) Roth, *R. gelida* (Geitzenauer) Backman, *R. pseudoumbilica* (Gartner) Gartner, *S. moriformis* (Brönnimann and Stradner) Bramlette and Wilcoxon, *Umbilicosphaera jafari* Müller. Discoasterids are scarce and represented by *D. deflandrei* Bramlette and Riedel, *D. exilis* Martini and Bramlette, *D. musicus* Stradner, and *D. variabilis* Martini and Bramlette.

Helicosphaera waltrans Theodoridis, whose restricted stratigraphic range was described by Fornaciari et al. (1996) and Abdul Aziz et al. (2007) from the Mediterranean area, is present in Lower Badenian sections from the localities Frättingsdorf and Niederleis (northern Vienna Basin). The absence of this species and the presence of *S. heteromorphus* allows an attribution of the investigated core into the upper part of nannoplankton Zone NN5 (Langhian, see Fig. 2), corresponding with the Upper Lagenid Zone. The stratigraphic interval of *H. waltrans* is correlated with the Lower Lagenid Zone (Švábenická 2002; Ćorić et al. 2007).

Foraminifera

The rare to common occurrence of species stratigraphically important for the Parathethys such as *Uvigerina grilli* Schmid, *Vaginulina legumen* (Linnè), *Praeorbulina glomerosa*

circularis (Blow), and *Orbulina suturalis* Brönnimann (Cicha et al. 1998) indicate a position within the lowermost part of the Upper Lagenid Zone (Early Badenian). An assignment of these microfaunas to the Mt6 Zone of Berggren et al. (1995) is problematic because *Globorotalia peripheroronda* Blow and Banner is, with the exception of a few, problematic specimens, missing in the sediments of the Vienna Basin. Unlike the upper 90 m of the core, the lowermost 10 m show microfaunas exclusively composed of longer-ranging taxa due to environmental changes and, therefore, cannot be attributed to either the Lower or the Upper Lagenid Zone.

According to the age of -14.74 my for the FO (first occurrence) of *Orbulina suturalis* as dated by Lourens et al. (2004a, b) and -14.561 ± 4 my (Abdul Aziz et al. 2007) the investigated core interval can be placed above this datum level. This is supported also by the absence of *H. ampliaperta* with LO (last occurrence) at -14.91 my (Lourens et al. 2004a, b).

Sequence stratigraphy

In a sequence stratigraphic framework, the succession at the borehole Baden-Sooss can be correlated to the lowermost third-order sequence of the Badenian in the Vienna Basin, sequence VB 5 or Ba1; this is correlated to the Lower Lagenid Zone and parts of the Upper Lagenid Zone (Kováč et al. 2004; Strauss et al. 2006). The top of this sea-level cycle has been correlated to the global -14.2 my hiatus by Strauss et al. (2006) and is associated with a major sea-level drop throughout the Vienna Basin (e.g. Weissenbäck 1996). However, the correlation of these regional sea-level cycles to the global sea-level curve (Haq et al. 1988) remains debatable, and no direct dating using global cycles has yet been achieved.

Sedimentology, carbonate and organic carbon content

The Badenian sediments in the western part of the southern Vienna Basin comprise mainly marly shales and silts, sands, and gravels. The sedimentary succession of the core consists of more than 95% marly shales and marls. The whole core is characterized by the presence of bioturbation (Fig. 3a). The main lithologies are bioturbated medium-to-dark gray marls and shales with carbonate contents (measured by Müller-Gastner bombs) between 11 and 25% and organic carbon (C_{org}; measured by LECO RC412) percentages between 0.35 and 0.65. Rare intercalations include up to 20-cm-thick bioturbated sand layers with some shell debris (mainly mollusks), an 80-cm-thick intraformational conglomerate (around 27 m) and a light

Fig. 3 Photograph of core slabs. **a** Strongly bioturbated marly shale facies; mainly ichnogenus *Phycosiphon* and *Palaeophycus* (core 17.0 m). **b** Laminated facies with low grade of bioturbation (core 84.5 m)
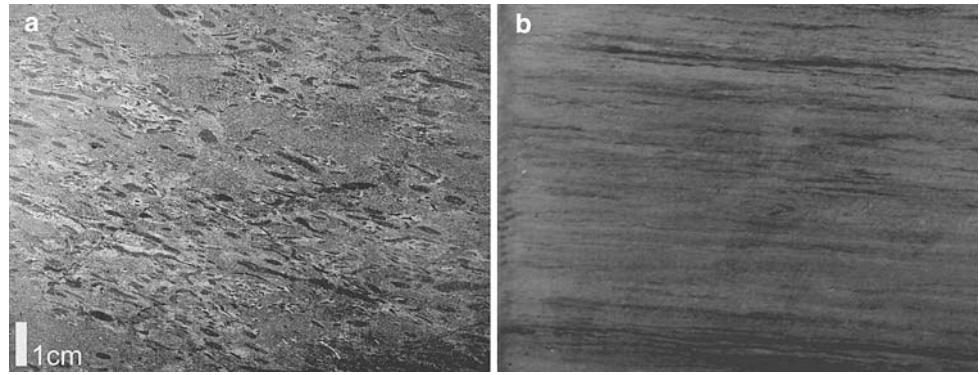
gray, 5-cm-thick tuff (at 72.3 m; Fig. 1). In the lower part of the core, around 80–85 m, light-dark laminated inter-calations with minor bioturbation are present (Figs. 1, 3b).

Grain-size distributions were determined using a sedigraph analyzer. Overview samples taken from depths of 20, 40, 60, 80, and 100 m of the core indicate a very uniform grain-size distribution (Fig. 4). The sediment is a mixture of clay and silt particles, mainly silty clays and fine silts. Only a very small portion (maximum 1.5%) of the sediments falls into the sand size fraction. The sorting is rather poor. No distinct grain size trend is recognizable from top to bottom. The results of overview XRD samples indicate quartz, muscovite/illite, chlorite, smectite, potash feldspar, and calcite as the main mineral constitutes. Minor peaks indicate the presence of pyrite.

Ichnology

Except for several layers with primary laminations, the core is completely bioturbated. Trace fossils from the ichnogenera *Chondrites*, *Ophiomorpha*, *Nereites*, *Phycosiphon*, *Scolicia*, *Siphonichnus*, *Teichichnus*, *Thalassinoides*, *Trichichnus*, and *Zoophycos* can be distinguished in cross-section. *Phycosiphon* dominates the core (Fig. 3a), occurs in nearly all horizons and is accompanied in many layers by *Nereites*. Other trace fossils like *Scolicia*, *Trichichnus* and *Zoophycos* are concentrated in the deeper portion of the core. *Thalassinoides* is completely absent in these deeper horizons, shows a maximum in the middle part and also occurs frequently in the upper core.
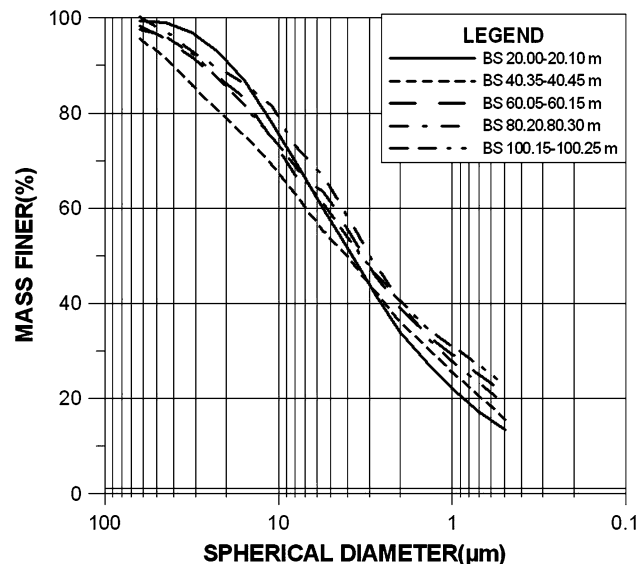
Although *Phycosiphon* has no connections to the sea floor, it is common in poorly oxygenated sediments (Ekdale and Mason 1988). This trace fossil is interpreted as a structure originating from deposit feeding and indicates a high portion of particulate organic matter in the sediment. *Trichichnus* typically has a strong tendency to pyritization. It is a deep-tier trace fossil, produced by opportunistic organisms in poorly oxygenated sediments (McBride and Picard 1991), perhaps by chemosymbiotic meio-infauna. *Zoophycos* and *Chondrites* are typical members of soft bottom communities settling in muddy, organic-rich, dys-aerobic sediments deposited under quiet conditions.

The trace fossil *Scolicia*, produced by irregular echinoids, indicates fully marine conditions (Bromley and Asgaard 1975; Smith and Crimes 1983). The salinity tolerant crustacean burrow *Thalassinoides* (Frey et al. 1984) replaces *Scolicia* in the higher portions of the core.

The distribution of trace fossils shows a tendency toward the upper part of the core indicated by the transition from the *Zoophycos* ichnofacies to a very distal *Cruziana* ichnofacies.

Palaeo- and rock-magnetic investigations

The rock- and palaeomagnetic investigations on the core included magnetic polarity and observations of cyclic variations of different magnetic parameters (see Selge 2005). Measurements included volume- and mass-specific susceptibility, anisotropy of magnetic susceptibility (AMS), natural remanent magnetization (NRM), alternating field

Fig. 4 Grain size curves (Sedigraph ET5100) of selected samples of the Baden-Sooss core from 20 to 100 m depth. Note uniform grain size trend within the whole core and significant portion of clay

(AF) demagnetization, isothermal remanent magnetization (IRM) and anhysteretic remanent magnetization (ARM). Additional detailed IRM component analysis and Curie-point determinations were carried out on selected samples (for detailed descriptions and instrument specifications see Selge 2005). Several magnetic parameters and ratios were calculated as a function of mineralogy, concentration, and grain size; this helped to interpret magnetic carrier minerals and cycles (Selge 2005).

No clear polarity pattern could be obtained due to very low initial NRM intensities and magnetic susceptibility values, indicating low concentrations of magnetic matter in the sediments, and due to the complex mineralogical composition. Although independent quality parameters were developed, the determination of the magnetic polarity stratigraphy from AF demagnetization component analysis failed. The magnetic properties of the sediments reflect the combined effects of mixed assemblages of multiple magnetic fractions with different grain sizes and mineralogy (such as magnetite, maghemite, hematite, goethite, pyrite, and possibly other iron sulfides).

Isothermal remanent magnetization acquisition curves component analysis and backfield experiments indicate a low-coercivity magnetic carrier mineral (magnetite) as the dominant magnetic phase. Two different populations of the low-coercivity component are present within the cyclic peak maxima (magnetite/maghemite). A high-coercivity component is present in all studied samples, indicating goethite/hematite. The results of thermomagnetic investigations also indicate magnetite as the dominant magnetic phase in all studied samples, with presence of some additional hematite and pyrite.

Periodicity

Spectral analyses

Magnetic susceptibility, calcium carbonate, and organic carbon content were studied with respect to periodicity. The upper part of the core (6–40 m) is tectonically disturbed, hampering the assumption of evenly time-spaced samples. The time series analyses therefore concentrated on the deeper, tectonically unaffected core (40–102 m). In this core part, homogeneous sediments indicate continuous sedimentation with rather constant sedimentation rates. For investigation of $CaCO_3$ and C_{org} content, samples were taken in 20-cm intervals, yielding 310 equally spaced samples; magnetic susceptibility measured in 5-cm intervals yielded 1,176 measurements for the lower part and 1,797 measurements for the total core.

Correlations between the three variables are extremely significant (Table 1), whereby the positive correlation between $CaCO_3$ and C_{org} is evident, and magnetic susceptibility is negatively correlated with both former characters.

To detect significant periods and cycles, spectral analysis was performed using the Lomb periodogram (Lomb 1976; Press et al. 2002; Hammer and Harper 2006). The power spectra are shown in Fig. 5 with a significance level of 1% error probability. Regarding the deeper core, coincidence of peaks with a period of 44.9 m are obvious in $CaCO_3$ and magnetic susceptibility, while in the organic carbon spectrum the first dominant peak indicates a period of 35.3 m. In both calcium carbonate and organic carbon spectra, the second significant peak characterizes a period of 22.5 m, while in the spectrum of magnetic susceptibility a shorter period (20.9 m) is evident. Again, a third peak with a period of 15.5 m is identical in both calcium carbonate and organic carbon (significant in the latter with 5% error probability), while in the power spectrum of magnetic susceptibility a similar peak characterizes a slightly shorter period (14.5 m). Coincidence between organic carbon and magnetic susceptibility occurs in the last significant peak at a period of 11.2 m. A comparable, but insignificant peak is located in $CaCO_3$, indicating a period of 10.7 m, inconsiderably shorter than in both other power spectra. Only the magnetic susceptibility spectrum with a higher resolution (5 cm intervals) shows a final significant peak at a period of 7.6 m.

Although power spectra demonstrate high correspondence in period lengths between $CaCO_3$, C_{org}, and magnetic susceptibility, their phases must be different according to the correlation coefficients in Table 1. Cross-correlations (Davis 2002) determine intensities in phase shifts (Fig. 6). The shift between magnetic susceptibility and calcium carbonate (22.2 m) is approximately half of the largest period (44.9 m) found in both power spectra, confirming the high-negative correlations. Phase differences of 3.2 m between calcium carbonate and organic carbon are marked by a significantly higher positive correlation ($r = 0.680$) at lag 16 compared to $r = 0.459$ at lag 0 in Table 1.

Table 1 Correlation between organic carbon, calcium carbonate and magnetic susceptibility in the deeper core (40–102 m)

	C_{org}		Magnetic susceptibility	
$CaCO_3$	Correlation	0.4588	Correlation	−0.7677
	Probability H_0	*7.56E-18*	*Probability H_0*	*8.95E-62*
C_{org}			Correlation	−0.4186
			Probability H_0	*6.99E-15*

Arcsine root-transformation (Linder and Berchtold 1976) of $CaCO_3$ and C_{org} percentages before calculating linear correlation

Comparing the power spectra of magnetic susceptibility at the deeper part with the complete drill reveals differences (Fig. 5). While in the complete core the period characterized by the first peak is shorter (40.3 m) than in the deeper part (period: 44.9 m), the period indicated by the second peak is longer (23.2 m) in the complete drill versus the deeper part (20.9 m), also longer than the 22.5 m of the $CaCO_3$ and C_{org} spectra. The following peak in magnetic susceptibility of the deeper drill part, indicating a period of 14.5 m, is subdivided in the complete core into two peaks with 12.7 and 11.1 m periods. The third peak in the spectrum of the deeper core, indicating a period of 11.2 m, corresponds to the bimodal peak (8.7 and 8.1 m) in the spectrum of the complete drill. This hints at time compression due to disturbed sedimentation of the upper drill part compared to the unaffected deeper part.

Regarding the power spectrum of magnetic susceptibility of the upper part of the core, the absence of the ~ 40 m period is evident. The peak indicating a period of 25.3 m is followed by significant peaks at 12.1 and 8.2 m (Fig. 5), followed by two peaks at 6.2 and 4.5 m that are significant with 5% error probability.

Relating the four significant periods in magnetic susceptibility of both core parts, which is confirmed by similar amplitudes in the frequency distributions, yields an average shortening of periods in the upper core to 56.5%. This reduction may reflect the intensive tectonics visible in the upper core.

Decomposition of periodic functions

Power spectra allow the recognition of cycles with fixed durations, but the position of their peaks along the axis representing time (like core meters) remains unknown, especially in profiles with disturbed or incomplete sedimentation. The wavelet transform (e.g. Torrence and Compo 1998; Guyodo et al. 2000) was used to obtain the position of cycle peaks along the core, whereby the mother wavelet was set to Morlet (e.g. Morlet et al. 1982; Hammer and Harper 2006). In the wavelet scalograms of Figs. 7, 8 and 9, the vertical axes represent core meters, while in the horizontal axes the number of samples within a period is shown as exponents to the base 2. Gray scales indicate the intensity of cycles and their position around a particular time (core meter). Positions of intensity spots parallel to the vertical axis point to fixed cycle periods, while scattered spots signalize cycles with changing periods.

Fig. 5 Power spectra (Lomb periodogram) of calcium carbonate, organic carbon and magnetic susceptibility (*dashed line* 1% error probability)
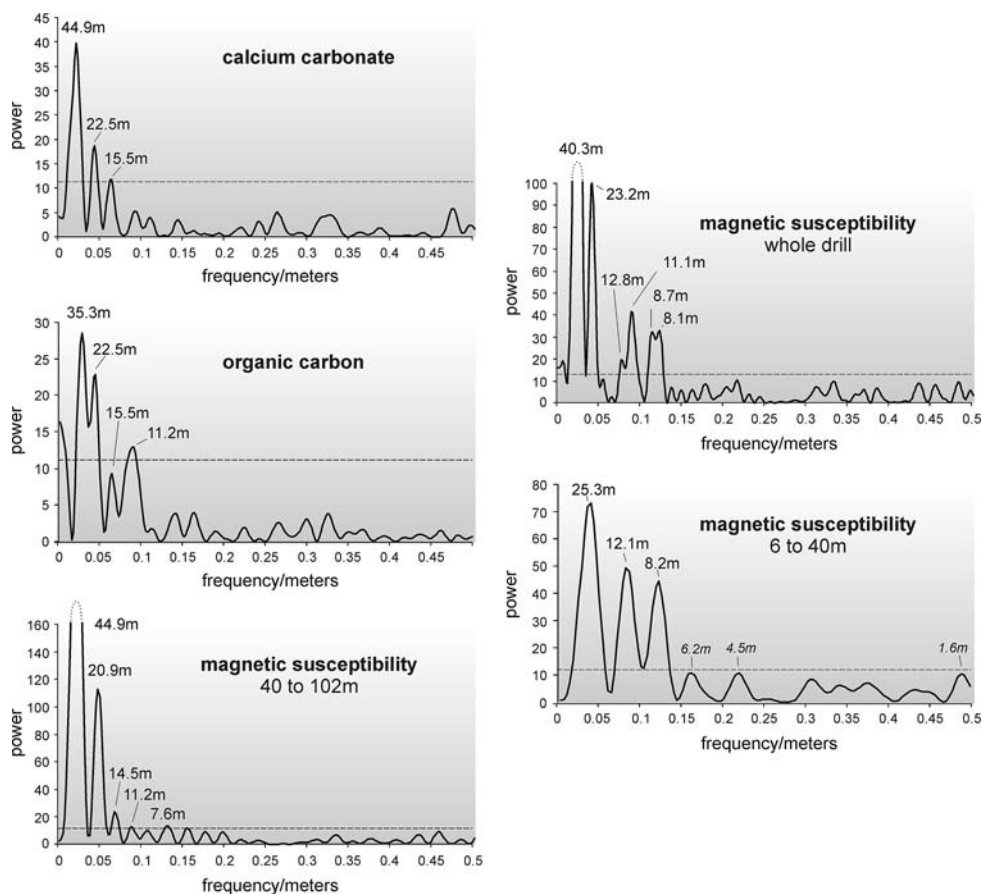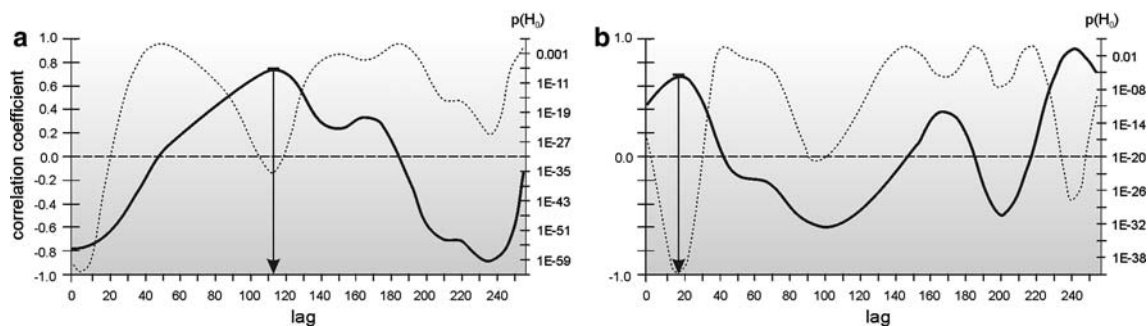
Fig. 6 Cross-correlations between calcium carbonate and magnetic susceptibility (**a**) and between calcium carbonate and organic carbon (**b**). Lag width = 0.2 m; *thick lines* correlation coefficient, *dashed lines* probability of non-correlation. *Arrows* point to most highly significant correlations

Using non-linear regression analyses (SPSS 2006), the periodic functions were decomposed into their significant components using

$$y = a_0 + \sum_{j=1}^{m} \left[a_j \cos \left(2\pi/l_j \right) \left(x - x_{0j} \right) \right] \quad \text{with } l_j > l_{j+1},$$
(1)

where a_0 is the mean level, a the amplitude, l the period and x_0 the acrophase of the jth component. The values of periods l_j are obtained from spectral analyses (Table 2).

The scalogram of organic carbon (Fig. 7) shows the best linear arrangement of density centers along the core axis, where the one series of density centers exactly corresponds to the 22.5 m period (number of measurements $2^s = 2^{6.81}$) and the other series parallels the 11.2 m period ($2^s = 2^{5.81}$) of the power spectrum (Fig. 5). Using decomposed periodic functions, the peaks of the three functions with narrower periods coincide significantly with density spots in wavelet analyses (Fig. 7).

The scalogram of calcium carbonate is similar to that of organic carbon, strengthening the high correlation by identical second and third peaks in the power spectra (Fig. 5). Nevertheless, the wavelet transform shows slight differences in the scale $s = 6.27$ (period of 15.5 m). Also, the fourth significant cycle differs between organic carbon and CaCO₃, where the six constant periods in the former are compressed in the deeper three periods of the latter; therefore, density points lay below the 10.5-m period line indicated by the power spectrum, and widened in the upper period (density points above the 10.5 m line; Fig. 8). These inconsistencies in period length are also expressed in the incongruence between positions of density points in the scalogram and their corresponding peaks in decomposed periodic components. Distances between peaks of similar wavelength are shorter in the deeper and slightly longer in the upper part of the scalogram (Fig. 8).

Due to incomplete sedimentation in the upper core, two independent wavelet analyses were performed (Fig. 9) for magnetic susceptibility. The scalogram of the deeper core shows incongruence with decomposed periodic functions, similar to calcium carbonate. Although the number of density points in the scalogram coincides with peak numbers of decomposed functions at every period level, they are not evenly distributed in the Morlet wavelets. This indicates fluctuating sedimentation rates. This contrast is strengthened in the upper core, where there are only a few coincidences between function peaks and density points, despite peak and spot numbers being identical in all functions (Fig. 9). The time compression of the upper core is visible in both scalograms and decomposed periodic functions (Fig. 9).

Comparing the three components with largest periods clearly demonstrates high congruence in all period lengths

Table 2 Parameter values of component functions (Eq. 1)

	Mean level	Amplitude	Period	Acrophase
Organic carbon				
Component 1	0.54	0.028	35.3	61.7
Component 2		0.028	22.5	51.6
Component 3		0.016	15.5	51.7
Component 4		0.026	11.2	46.1
CaCO₃				
Component 1	18.74	1.505	44.9	65.7
Component 2		0.704	22.5	56.1
Component 3		0.699	15.5	53.0
Component 4		0.582	10.7	52.5
Magnetic susceptibility 40–102 m				
Component 1	157.17	21.05	44.9	43.7
Component 2		9.595	20.9	44.8
Component 3		3.389	14.5	48.8
Component 4		3.951	11.2	44.6
Magnetic susceptibility 6–40 m				
Component 1	148.84	21.261	25.3	16.3
Component 2		12.004	12.1	12.7
Component 3		11.390	8.2	16.9
Component 4		4.415	6.2	7.3

Fig. 7 Organic carbon: **a** frequency diagram and fit by a composite periodic function reduced to four components (Table 2). **b** Scalogram (wavelet transform) based on the Morlet wavelet; *lines* along density points obtained by significant period lengths of the power spectrum in Fig. 5. **c** Graphs of single component functions (Table 2) oscillating around the mean level

between magnetic susceptibility and $CaCO_3$: in all functions the phase shift is half of the period length (Fig. 10). This confirms the complementary reaction of both parameters to periodically changing environmental conditions. The slight shift between calcium carbonate and organic carbon as demonstrated by cross correlation (Fig. 6) can

now be shown in phase shifts of the shorter periodic functions with identical period lengths (Fig. 10b, c). On the other hand, the phase shift of the function with the largest period is distinct in the deeper part of the deeper core and blurred in its upper part by the shorter period (Table 2, Fig. 10a).
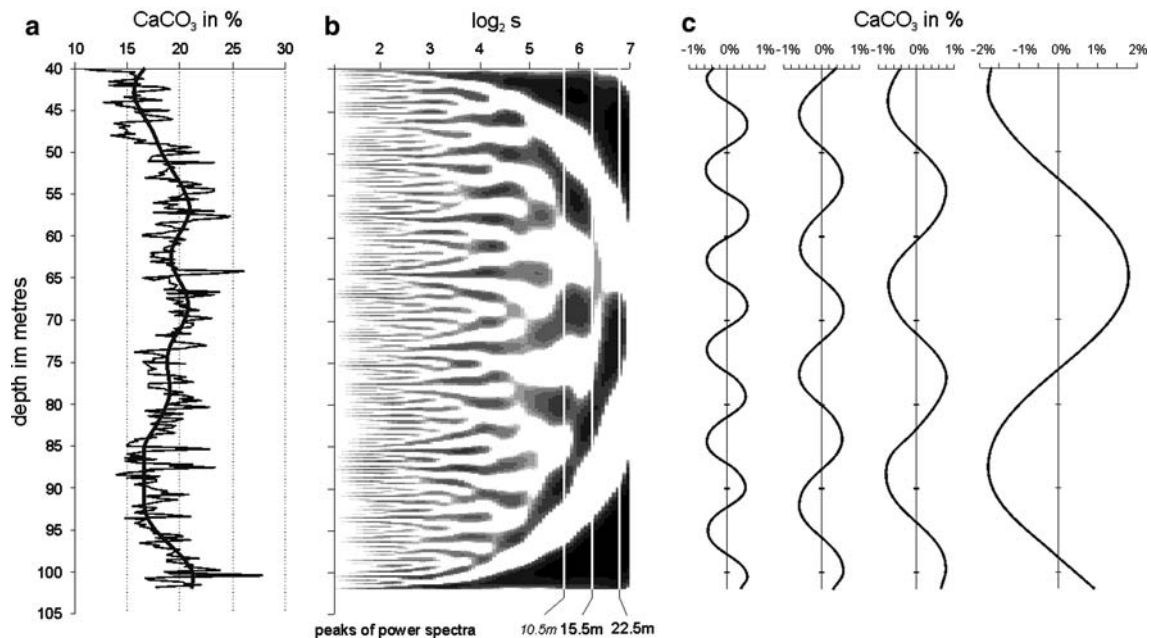
Fig. 8 Calcium carbonate: **a** frequency diagram and fit by a composite periodic function reduced to four components (Table 2). **b** Scalogram (wavelet transform) based on the Morlet wavelet; *lines* along density points obtained by significant period lengths of the power spectrum in Fig. 5. **c** Graphs of single component functions (Table 2) oscillating around the mean level

Phase relations

The four significant periods of organic carbon, calcium carbonate and magnetic susceptibility were correlated with the following three sequences of orbital cycles:

Sequence 1	400, 100, 41 and 23 kyr
Sequence 2	100, 41, 23 and 19 kyr
Sequence 3	41, 23 and 19 kyr

based on the regression $y = ax$ running through the origin (Zar 1999), where y represents the period length in meters and x the orbital cycle length in kyr (Fig. 11). In CaCO$_3$ and magnetic susceptibility (deeper core), core periods significantly correlate with orbital cycles starting with 100-kyr eccentricity as the largest. Other correlations equalizing sequences of the core with orbital cycles starting at 400 or 41 kyr are less or non significant. Insignificance in the correlation of C$_{org}$ spectra (Table 3) with the sequences starting at 100 kyr reflects the much shorter first period in the core (35.3 m) compared with 44.9 m in both other spectra (Fig. 5). Therefore, the four cycles in the Baden-Sooss core can be correlated with the 100, 41, 23, and 19 kyr Milankovich cycles.

According to the high-positive correlation between magnetic susceptibility and orbital cycles, especially eccentricity and obliquity (e.g. Yamazaki and Oda 2002; Mader et al. 2004; Latta et al. 2006; Ohneiser et al. 2006; Schmieder 2006), phases in both larger cycles of magnetic susceptibility can be correlated with orbital cycles. The 100-kyr eccentricity and 41-kyr obliquity peaks could be
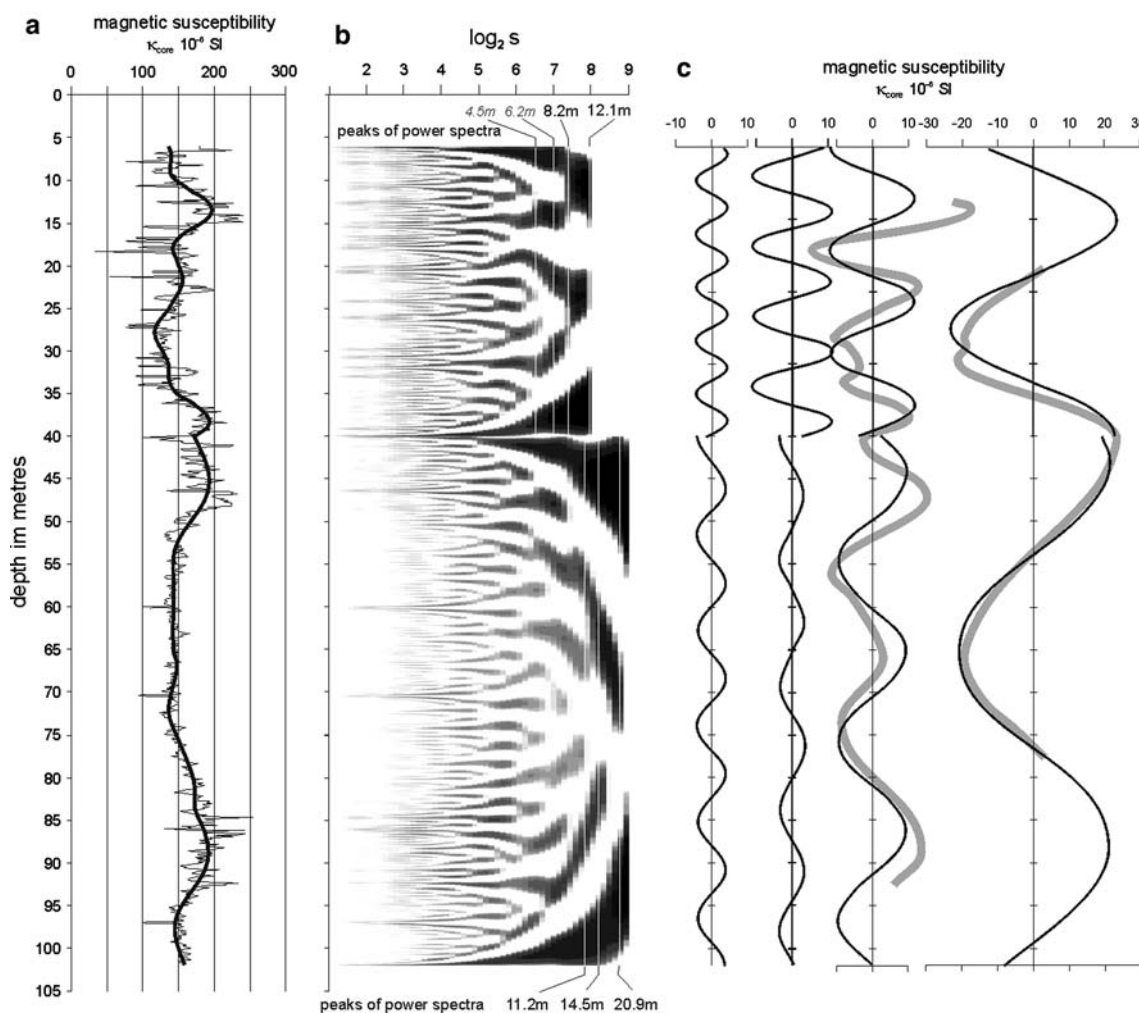
Fig. 9 Magnetic susceptibility of the complete core: **a** frequency diagram and fit by a composite periodic function reduced to four components (Table 2). **b** Scalogram (wavelet transform) based on the Morlet wavelet; *lines* along density points obtained by significant period lengths of the power spectrum in Fig. 5. **c** Graphs of single component functions (Table 2) oscillating around the mean level. *Grey lines* indicate a posteriori filtered harmonics equalizing function periods with 97 kyr eccentricity and 41 kyr tilt cycles (explanation in the text)

Fig. 10 Comparison of the three decomposed periodic functions with largest periods; amplitudes set to identical heights
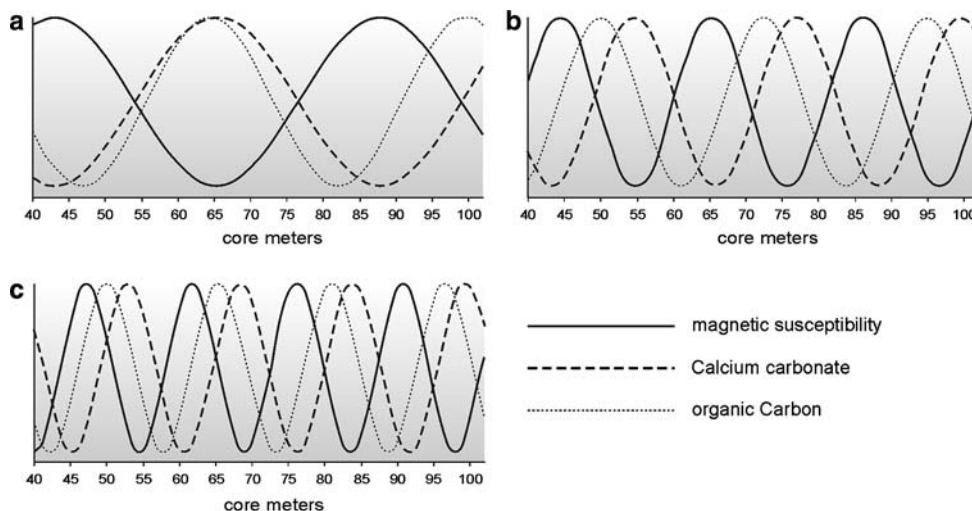
equalized with peaks of magnetic susceptibility because the maxima of magnetic parameters (magnetic susceptibility and NRM intensity) can be linked to higher concentrations of magnetic matter due to the increased sedimentary influx. This can be explained by seasonal contrasts as induced by increased eccentricity or obliquity. The result is higher rates of physical weathering and erosion and thus an increased amount of detrital magnetic particles deposited in the basin. This is confirmed by the hematite concentration proxy IRM@AF (e.g. Larrasoana et al. 2003) and the HIRM, which show the highest values within the peak maxima, indicating the increased contribution of hematite. These can be related to the deposition by eolian and fluviatile processes in such marine environments. Several other parameters and ratios (e.g. ARM, K_{ARM}, ARM/ SIRM, K_{ARM}/K_{mean}, ARM/K_{mean}; see Selge 2005) also indicate a higher amount of coarse-grained particles due to the increased detrital input during eccentricity or obliquity maxima. Cycle minima characterize periods of lower detrital input, when the magnetic properties were mainly dominated by fine-grained biogenic and authigenic particles formed during diagenesis (for parameters see Deng et al. 2005).

Transferring the core distance between 40 and 102 m into time differences by equalizing the second cycle (period of 20.9 m) with obliquity, then the time span of the lower core is 121.3 kyr. Since the upper core (8–40 m) is tectonically compressed to $\sim 57\%$, decompression and time relation yield an interval of approximately 116 kyr for the upper part.

Astronomical tuning

For an exact dating of the deeper core, the two sinus waves of magnetic susceptibility with largest periods were divided into sections of 2 kyr. These time-calibrated waves obtained from the core can now be simultaneously cross-correlated with the 100- and 41-kyr orbital cycles as calculated by Laskar et al. (2004). To obtain normalized
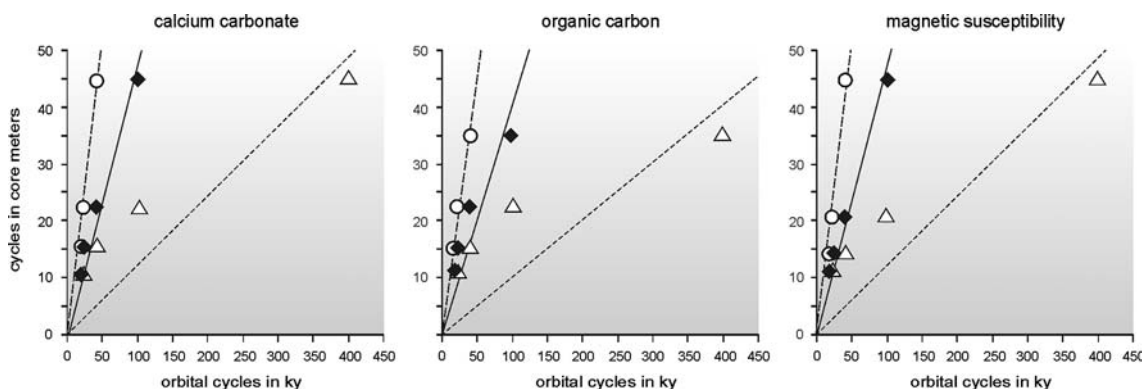
Fig. 11 Regression of the four largest periods in geochemical and geomagnetic variables on orbital cycles

Table 3 Cross correlation and linear regression running through the origin between significant periods in the power spectra of calcium carbonate, organic carbon, and magnetic susceptibility (40–102 m) on the one side and orbital cycles on the other (significant correlations in bold)

Correlation of periods equalizing the largest core period with (kyr)	Calcium carbonate		Organic carbon		Magnetic susceptibility (40–102 m)	
400	Regression coefficient	0.1225	Regression coefficient	0.1002	Regression coefficient	0.1220
	Correlation	0.7564	Correlation	0.4047	Correlation	**0.8266**
	Probability H₀	*0.1218*	*Probability H₀*	*0.2976*	*Probability H₀*	*0.0422*
100	Regression coefficient	0.4751	Regression coefficient	0.3995	Regression coefficient	0.4688
	Correlation	**0.9707**	Correlation	0.8147	Correlation	**0.9813**
	Probability H₀	*0.0146*	*Probability H₀*	*0.0926*	*Probability H₀*	*0.0094*
41	Regression coefficient	1.0319	Regression coefficient	0.8788	Regression coefficient	1.0102
	Correlation	0.9730	Correlation	0.9820	Correlation	0.9607
	Probability H₀	*0.0741*	*Probability H₀*	*0.0605*	*Probability H₀*	*0.0896*

amplitudes for orbital cycles, both curves have been filtered using a modified harmonic filtering algorithm (Ferraz-Mello 1981) centered for eccentricity at 0.01 kyr^{-1} with 0.003 kyr^{-1} bandwidth, and centered for obliquity at 0.024 kyr^{-1} with 0.008 kyr^{-1} bandwidth (Schulz et al. 1999). In combined cross correlation, the lag width is 2 kyr; the comparison starts with the younger (upper) limit of the core (Fig. 12).

Filtering 97- and 41-kyr cycles from the time-calibrated frequency distribution of magnetic susceptibility of the complete core demonstrates high congruence between the decomposed frequency distributions and filtered harmonics using period lengths of orbital cycles. This confirms the correctness of time calibration (Fig. 9). Referring to former stratigraphic positioning of the Badenian (Strauss et al. 2006), the investigated time span of the reference section could be reduced to the interval between −15.0 and −13.8 my, although cross correlation was calculated down to −16 my. The highest correlation ($r = 0.961$, $n = 122$) was found at lag 229. This corresponds to the time interval from −14.379 to −14.258 my (Fig. 12). A second, highly significant interval ($r = 0.954$) at lag 49 spans the time between −14.019 and −13.898 my. The third correlation peak ($r = 0.918$ at lag 409) marks the interval from −14.739 to −14.618 my (Fig. 12).

Using the data based on magnetic susceptibility for the upper core, we detected a reduction of periods to ∼57% for all cycles (see above). Therefore, the decompression of the 34-m upper core length corresponds to a time interval of 116 kyr. Summing up the two time intervals yields ∼238 kyr for the whole core; this represents two eccentricity cycles, which are found in the frequency diagram of magnetic susceptibility (Fig. 9).

The three intervals with highest correlation were compared to find tie points for dating. Biostratigraphically, the whole core belongs to the NN5 Zone: It must therefore be younger than −14.9 my. *Helicosphaera waltrans*, typical and abundant in the Lower Lagenid Zone, is absent in the whole core, but present in other locations of the Vienna Basin (Rögl et al. 2007). Since the LCO (last common occurrence) of *H. waltrans* is dated in the Mediterranean at around −14.357 my (Abdul Aziz et al. 2007), the interval from −14.739 to −14.618 my must be excluded.

Strauss et al. (2006) found in the Vienna Basin a distinct sequence boundary, documented by a hiatus, between the Upper Lagenid and the *Spiroplectammina* Zone. They positioned this event at −14.2 my (Shevenell et al. 2004) prerunning the cooling event caused by the Antarctic ice shield at −13.9 my (Holbourn et al. 2005). Since only a slight shallowing tendency can be assumed due to the higher sedimentary input (expressed in higher magnetic susceptibility and a few sandy intercalations in the upper core), we must also reject the positioning of the younger interval (−14.019 to −13.898 my), exactly before the cooling period.

Based on the above results, including the time extension represented in the upper core, we verified the dating of the Baden-Sooss core between −14.379 ± 1 and −14.142 my ± 9 kyr. The younger (upper) boundary shows a wider confidence limit compared to the core base due to estimation error. This estimation is supported by 40Ar/39Ar dating within the Lower Lagenid Zone of the Styrian Basin (with abundant *H. waltrans*), yielding −14.39 ± 0.12 my (Handler et al. 2006).

Conclusion

The equalization of the significant cycles obtained by power spectra analyses based on magnetic susceptibility, calcium carbonate and organic carbon with eccentricity (100 kyr), obliquity, and precession cycles is supported by sediment accumulation rates. This yields an averaged rate of 0.45 mm year^{-1} for the tectonically unaffected deeper

Fig. 12 Cross-correlation diagram between time-calibrated significant waves of the core and harmonically filtered orbital cycles (Laskar et al. 2004) as the reference section in the interval −15.0 to −13.8 my
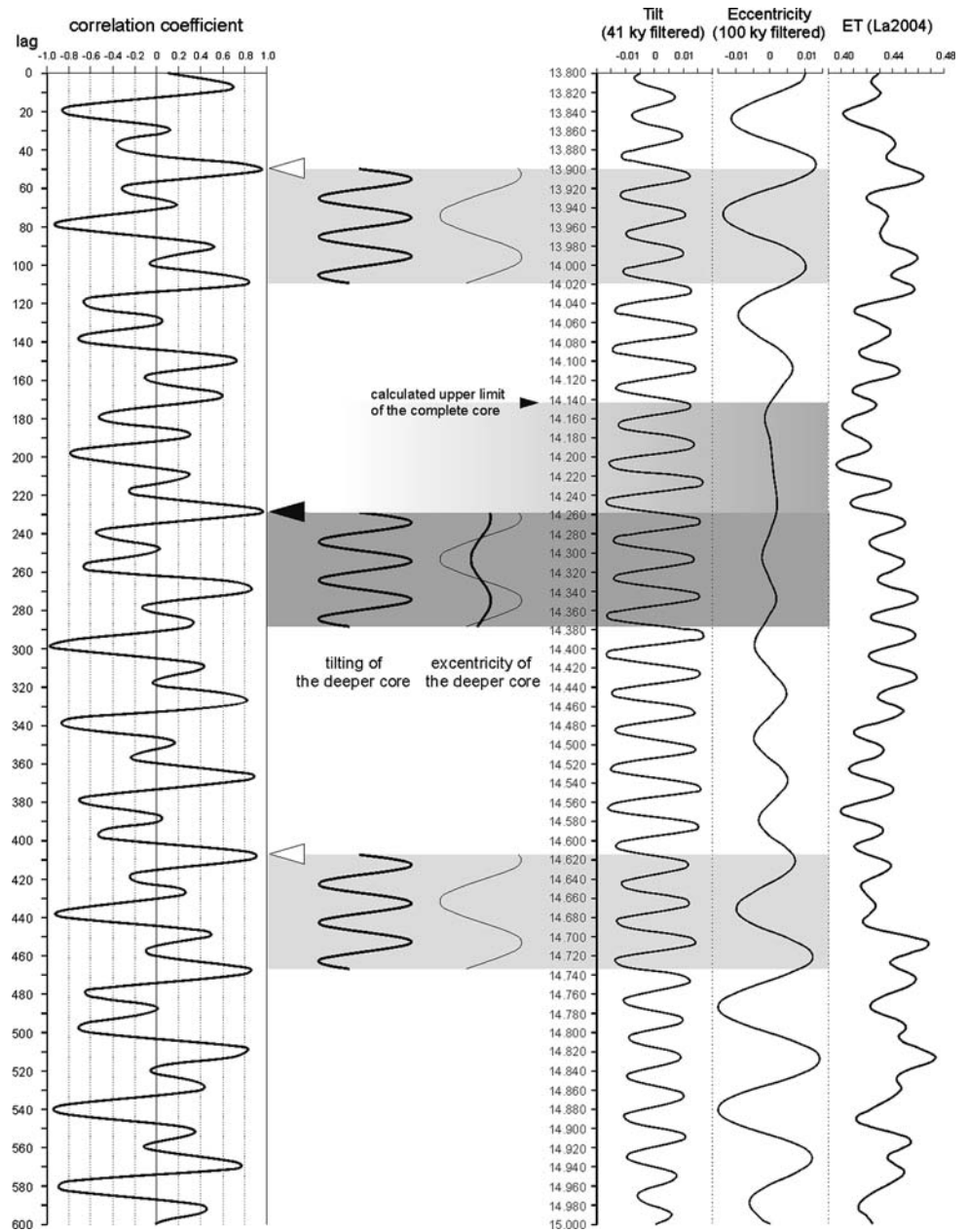
core (40–102 m). According to the lateral position of the borehole in the southern Vienna Basin, this rate is of similar (slightly lower) range to the averaged sediment accumulation rate of 0.56 mm year^{-1} in the Lower and Upper Lagenid Zone in the center of the southern basin (OMV drill Sollenau 1; Brix and Plöchinger 1988).

Cross correlation (lag width: 2 kyr) of phase-related periods in magnetic susceptibility with orbital cycles (La2004) started at −13.8 my and ended at −15.9 my, thus spanning the whole time interval between −16.0 and −13.8 my as suggested by biostratigraphy. Beside the highest correlation, the assignment of the core between

−14.379 ± 1 and −14.142 my ± 9 kyr is supported by the lack of *H. ampliaperta* Bramlette and Wilcoxon (LO: −14.91 my from Lourens et al. 2004a, b), and by the lack of the succeeding *H. waltrans* Theodoridis with a LCO at ~14.357 my (Abdul Aziz et al. 2007). The latter could not be an ecological or paleogeographical effect because *H. waltrans* is represented in the Lower Lagenid Zone of the Vienna Basin (Rögl et al. 2007).

In the case of the LCO of *H. waltrans* at ~14.357 my, the statistically significant interval from −14.739 to −14.618 my has to be excluded for time allocation of the undisturbed drill part. The youngest significant interval

(extended by the upper core ranging from −14.019 to −13.781 my) coincides with the Middle Miocene cooling and must therefore also be excluded.

Obliquity cycles that mainly affect the climate in the eligible interval between −14.4 and −14.1 my are reflected in magnetic susceptibility, trace fossils, and foraminiferal fauna. Magnetic susceptibility is low in the deeper core and intensifies toward the upper part, possibly caused by slight shallowing tendencies. The increased input of terrestrial detritus in the upper part causes transition from a *Zoophycos* to a *Cruziana* ichnofacies. Planktonic and benthic warm-water foraminifera (e.g. *Globigerinoides quadrilobatus/sacculifer*, *Paragloborotalia mayeri/siakensis*, *Lenticulina ariminensis*, *L. echinata*) are abundant and large in the Lower Lagenid Zone and more rare and smaller in the Upper Lagenid Zone, again showing the influence of orbital cycles (Fig. 12).

Therefore, the time interval between −14.379 and −14.142 my is the most probable position of the scientific drill core Baden-Sooss according to biostratigraphic and palaeoenvironmental data. This allows, for the first time, a cyclostratigraphic dating of parts of the Badenian stage in the Vienna Basin.

References

Abels HA, Hilgen FJ, Krijgsman W, Kruk RW, Raffi I, Turko E, Zachariasse WJ (2005) Long-period orbital control on middle Miocene global cooling: integrated stratigraphy and astronomical tuning of the Blue Clay Formation on Malta. Paleoceanography 20. doi:10.1029/2004PA001129

Abdul Aziz H, Di Stefano A, Foresi LM, Hilgen FJ, Iaccarino SM, Kuiper KF, Lirer F, Salvatorini G, Turco (2007) Integrated stratigraphy and 40Ar/39Ar chronology of early Middle Miocene sediments from DSDP Leg 42A, Site 372 (Western Mediterranean). Palaeogeogr Palaeoclimatol Palaeoecol (in press)

Baldi K, Hohenegger J, Rögl F, Rupp C, Pervesler P, Khatun M (2005) Ecology of benthic foraminifera in the drill section of the Badenian Stratotype at Baden-Soos (Middle Miocene, Lower Austria). In: 12th Congress RCMNS, 6–11 September 2005, Vienna, Abstract volume: 15–17

Berggren WA, Kent DV, Swisher CC III, Aubry M-P (1995) A revised Cenozoic geochronology and chronostratigraphy. Society of Sedimentary Geology (SEMP). Spec Publ 54:129–212

Brix F, Plöchinger B (1988) Erläuterungen zu Blatt Wiener Neustadt. Geol Bundesanst 1–85

Bromley RG, Asgaard U (1975) Sediment structures produced by a spatangoid echinoid: a problem of preservation. Bull Geol Soc Den 24:261–281

Cicha I, Senes J (1968) Sur la position du Miocene de la Paratethys Central dans les cadre du Tertiaire de l'Europe. Geol Zbornik Geol Carp 19:95–116

Cicha I, Rögl F, Rupp C, Ctyroka J (1998) Oligocene–Miocene foraminifera of the Central Paratethys. Abh Senckenberg-naturforsch Ges 549:1–325

Ćorić S, Švabenicka L, Rögl F, Petrova P (2007) Stratigraphical position of *Helicosphaera waltrans* nannoplankton horizon (NN5, Lower Badenian) Joannea. Geologie und Paläontologie 9:17–19

Davis JC (2002) Statistics and data analysis in geology, 3rd edn. Wiley, New York, 639 pp

Decker K (1996) Miocene tectonics at the Alpine–Carpathian junction and the evolution of the Vienna Basin. Mitt Ges Geol Bergbaustud Österr 41:33–44

Decker K, Peresson H (1996) Tertiary kinematics in the Alpine–Carpathian–Pannonian system: links between thrusting, transform faulting and crustal extension. In: Wessely G, Liebl W (eds) Oil and gas in Alpidic thrustbelts and basins of Central and Eastern Europe. EAGE Spec Publ 5:69–77

Deng C, Vidic NJ, Verosub KL, Singer MJ, Liu Q, Shaw J, Zhu R (2005) Mineral magnetic variation of the Jiaodao Chinese loess/paleosol sequence and its bearing on long-term climatic variability. J Geophys Res 110:B03103

Ekdale AA, Mason TR (1988) Characteristic trace–fossil association in oxygen-poor sedimentary environments. Geology 16:720–723

Ferraz-Mello S (1981) Estimation of periods from unequally spaced observations. Astron J 86:619–624

Fornaciari E, Di Stefano A, Rio D, Negri A (1996): Middle Miocene quantitative calcareous nannofossil biostratigraphy in the Meditterranean region. Micropaleontology 42:37–63

Frey RW, Curran AH, Pemberton GS (1984) Tracemaking activities of crabs and their environmental significance: the ichnogenus *Psilonichnus*. J Paleontol 58:511–528

Fuchs R, Stradner H (1977) Über Nannofossilien im Badenien (Mittelmiozän) der Zentralen Paratethys. Beitr Paläont Österr 2:1–58

Fuchs T (1873) Erläuterungen zur geologischen Karte der Umgebung Wien. Geol Reichsanst Wien 1–47

Grill R (1941) Stratigraphische Untersuchungen mit Hilfe von Mikrofaunen im Wiener Becken und den benachbarten Molasseanteilen. Oel und Kohle 37:595–602

Grill R (1943) Über mikropaläontologische Gliederungsmöglichkeiten im Miozän des Wiener Beckens. Mitt Reichsamt Bodenforsch Wien 6:33–44

Guyodo Y, Gaillot P, Chanell JET (2000) Wavelet analysis of relative geomagnetic paleointensity at ODP Site 983. Earth Planet Sci Let 5666:1–15

Hammer Ø, Harper DAT (2006) Paleontological data analysis. Blackwell, Malden, 351 pp

Hamilton W, Wagner L, Wessely G (2000) Oil and gas in Austria. Mitt Österr Geol Ges 92:235–262

Handler R, Ebner F, Neubauer F, Hermann S, Bojar A-V, Hermann S (2006) 40Ar/39Ar dating of Miocene tuffs from Styrian part of the Pannonian Basin: an attempt to refine the basin stratigraphy. Geol Carpathica 57:483–494

Haq BU, Hardenbol J, Vail PR (1988) Mesozoic and Cenozoic chronostratigraphy and cycles of sea-level changes. In: Wilgus CK et al (eds) Sea-level changes—an integrated approach. SEMP Spec Publ 42:71–108

Hilgen FJ, Krijgsman W, Langereis CG, Lourens LJ, Santarelli A, Zachariasse WJ (1995) Extending the astronomical (polarity) time scale into the Miocene. Earth Planet Sci Let 136:495–510

Hilgen FJ, Krijgsman W, Raffi I, Turco E, Zachariasse WJ (2000) Integrated stratigraphy and astronomical calibration of the Serravallian/Tortonian boundary section at Monte Gibiscemi (Sicily, Italy). Mar Micropaleontol 38:181–211

Holbourn A, Kuhnt W, Schulz M, Erlenkeuser H (2005) Impacts of orbital forcing and atmospheric carbon dioxide on Miocene ice-sheet expansion. Nature 438:483–487

Khatun M, Selge A, Hohenegger J, Wagreich M, Stingl K, Scholger R, Pervesler P, Rupp C (2005) Cyclostratigraphy in the Middle Miocene (Lower Badenian) of the southern Vienna Basin. Geophys Res Abstr 8:00840

Kováč M, Baráth I, Harzhauser M, Hlavatý I, Hudáčková N (2004) Miocene depositional systems and sequence stratigraphy of the Vienna Basin. Cour Forsch-Inst Senckenberg 246:187–212

Larrasoana JC, Roberts AP, Rohling EJ, Winklhofer M, Wehausen R (2003) Three million years of monsoon variability over the northern Sahara. Clim Dyn 21:689–698

Laskar J, Robulet P, Joutel F, Gastineau M, Correia ACM, Levrard B (2004) A long-term numerical solution for the insolation quantities of the Earth. Astron Astrophys 428:261–285

Latta DK, Anastasio DJ, Hinnov LA, Elrick M, Kodama KP (2006) Magnetic record of Milankovitch rhythms in lithologically noncyclic marine carbonates. Geology 34:29–32

Linder A, Berchtold W (1976) Statistische Auswertung von Prozent-zahlen. UTB Birkhäuser Verlag, Basel, 232 pp

Lomb NR (1976) Least-squares frequency analysis of unequally spaced data. Astrophys Space Sci 39:447–462

Lourens L, Hilgen F, Shackleton NJ, Laskar J, Wilson D (2004a) The Neogene period. In: Gradstein FM, Ogg JG, Smith AG (eds) A geologic time scale 2004. Cambridge University Press, London, pp 409–440

Lourens L, Hilgen F, Shackleton NJ, Laskar J, Wilson D (2004b) Orbital tuning calibrations and conversions for the Neogene Period. In: Gradstein FM, Ogg JG, Smith AG (eds) A geologic time scale 2004. Cambridge University Press, London, pp 469–484

Mader D, Cleaveland L, Bice DM, Montanari A, Koeberl C (2004) High-resolution cyclostratigraphic analysis of multiple climate proxies from a short Langhian pelagic succession in the Cònero Riviera, Ancona (Italy). Palaeogeogr Palaeoclimat Palaeoecol 211:325–344

Martini E (1971) Standard tertiary and quarternary calcareous nannoplankton zonation. In: Proceedings of the II planktonic conference, Ed Tecnoscienza Roma, pp 739–785

Mayer-Eymar K (1858) Versuch einer neuen Klassifikation der Tertiär-Gebilde Europa's. Verhandlungen der allgem. Schweiz. Gesellschaft für die gesamten Naturwissenschaften bei ihrer Versammlung in Trogen 1857. J. Schläpfer, Trogen 70–71:165–199

McBride EF, Picard MD (1991) Facies implications of *Trichichnus* and *Chondrites* in turbidites and hemipelagites, Marnoso-aren-acea Formation (Miocene), Northern Apennines, Italy. Palaios 6:281–290

Morlet J, Arens G, Fourgeau E, Girard D (1982) Wave propagation and sampling theory. 2. Sampling theory and complex waves. Geophys 47:203–221

Ohneiser C, Wilson G, Field B, Crundwell M (2006) Evidence for orbital pacing through the middle Miocene climatic deterioration from the Southwest Pacific. Geophys Res Abstr 8:05421

Papp A, Cicha I, Seneš J, Steininger F (1978) Chronostratigraphie und Neostratotypen. Miozän der Zentralen Parathethys M4. Badenien. Chronostrat and Neostrat 6 (Bratislava), p 593

Papp A, Steininger F (1978) Holostratotypus des Badenien: Baden-Sooss. In: Papp A, Cicha I, Seneš J, Steininger F (eds) M4 Badenien (Moravien, Wielicien, Kosovien). Chronostrat and Neostrat 6:138–145 (Veda SAV, Bratislava)

Papp A, Turnovsky K (1953) Die Entwicklung der Uvigerinen im Vindobon (Helvet und Torton) des Wiener Beckens. J Geol Bundesanst 46:117–142

Papp A, Grill R, Janoschek R, Kapounek J, Kollmann K, Turnovsky K (1968) Zur Nomenklatur des Neogens in Österreich – Nomenclature of the Neogene of Austria. Verh Geol Bundesanst 1968:9–27

Piller WE, Harzhauser M (2005) The myth of the brackish Sarmatian Sea. Terra Nova 17:450–455

Piller WE, Egger H, Erhart CW, Gross M, Harzhauser M, Hubmann B, van Husen D, Krenmayr H-G, Krystyn L, Lein R, Lukeneder A, Mandl GW, Rögl F, Roetzel R, Rupp C, Schnabel W, Schönlaub HP, Summesberger H, Wagreich M, Wessely G (2004) Die stratigraphische Tabelle von Österreich 2004 (sed-imentäre Schichtfolgen)

Press WH, Teukolsky SA, Veterling WT, Flannery BP (2002) Numerical recipes in C++. Cambridge University Press, Cambridge, pp 580–589

Ratschbacher L, Frisch W, Linzer H-G, Merle O (1991) Lateral extrusion in the Eastern Alps, 2. Structural analysis. Tectonics 10:257–271

Rögl F, Ćorić S, Hohenegger J, Pervesler P, Roetzel R, Scholger R, Spezzaferri S, Stingl K (2007) Cyclostratigraphy and transgres-sions at the Early/Middle Miocene (Karpatian/Badenian) boundary in the Austrian Neogene basins (Central Parathethys). Austrian J. Earth Science (submitted)

Sauer R, Seifert P, Wessely G (1992) Guidebook to excursions in the Vienna Basin and the adjacent Alpine–Carpathian thrustbelt in Austria. Mitt Österr Geol Ges 85:1–264

Schaffer FX (1927) Der Begriff der "miozänen Mediterranstufen" ist zu streichen. Verh Geol Bundesanst 1927:86–88

Schmieder F (2006) Magentic signals in Plio–Pleistocene sediments of the South Atlantic: implications for chronostratigraphy and paleoceanography. Geophys Res Abstr 8:07269

Schulz M, Berger WH, Sarnthein N, Grootes PM (1999) Amplitude variations of 1470-year climate oscillations during the last 100,000 years linked to fluctuations of continental ice mass. Geophys Res Lett 26:3385–3388

Seifert P (1996) Sedimentary-tectonic development and Austrian hydrocarbon potential of the Vienna Basin. In: Wessely G., Liebl W (eds) Oil and gas in Alpidic thrustbelts and basins of Central and Eastern Europe. EAGE Spec Publ 5:331–341

Selge A (2005) Zyklostratigraphie anhand mineralmagnetischer Parameter am Bohrkern Sooß aus dem mittleren Badenium (Mittel Miozän)/Baden (Wiener Becken, Österreich). Dipl thesis, University of Leoben, 70 pp

Shevenell AE, Kenett JP, Lea DW (2004) Middle Miocene southern ocean cooling and Antarctic cryosphere expansion. Science 305:1766–1770

Smith AB, Crimes TP (1983) Trace fossils formed by heart urchins—a study of *Scolicia* and related traces. Lethaia 16:79–92

SPSS 15.0 for Windows (2006) Release 15.0.0. SPSS Inc.

Steininger FF, Wessely G (2000) From the Tethyan Ocean to the Parathethys Sea: Oligocene to Neogene stratigraphy, paleogeo-raphy and paleobiogeography of the circum-Mediterranean region and the Oligocene to Neogene basin evolution in Austria. Mitt Österr Geol Ges 92:95–116

Stradner H, Fuchs R (1978) Das Nannoplankton in Österreich. In: Papp A, Cicha I, Seneš J, Steininger F (eds) M4 Badenien (Moravien, Wielicien, Kosovien). Chronostrat and Neostrat 6:489–531 (Veda SAV, Bratislava)

Švábenická L (2002) Calcareous nannofossils of the upper Karpatian and lower Badenian deposits in the Carpathian Foredeep, Moravia (Czech Republic). Geol Carp 53:197–210

Strauss PE, Harzhauser M, Hinsch R, Wagreich M (2006) Sequence stratigraphy in a classic pull-apart basin (Neogene, Vienna Basin). A 3D seismic based integrated approach. Geol Carp 57:185–197

Torrence C, Compo G (1998) A practical guide to wavelet analysis. Bull Am Meteorol Soc 79:61–78

Wagreich M, Schmid HP (2002) Backstripping dip-slip fault histories: apparent slip rates for the Miocene of the Vienna Basin. Terra Nova 14:163–168

Weissenbäck M (1996) Lower to Middle Miocene sedimentation model of the central Vienna Basin. In: Wessely G, Liebl W (eds) Oil and gas in Alpidic Thrustbelts and Basins of Central and Eastern Europe. EAGE Spec Publ 5:255–363

Yamazaki T, Oda H (2002) Orbital influence on Earth's magnetic field: 100,000-year periodicity in inclination. Science 295:2435–2438

Zar JH (1999) Biostatistical analysis, 4th edn. Prentice-Hall, New Jersey, 63 pp